

Dynamic, Mechanical Efficiency and Fatigue Analysis of the Double Cardan Homokinetic Joint

M.E. Biancolini, C. Brutti, E. Pennestrì*, P.P. Valentini
Università di Roma Tor Vergata
Dipartimento di Ingegneria Meccanica
via del Politecnico, 1
00133 Roma - Italy

1 Introduction

Although the Cardan joint receives many industrial applications, its dynamics is not yet accurately described by the mathematical models found in technical literature. One of the most sophisticated modeling of the dynamics of such a joint has been presented in a series of papers authored by F. Freudenstein and his coworkers [1, 2, 3, 4].

In the named approach the analysis equations follow from the fundamental laws of rigid body mechanics. Thus, it cannot be applied to the real topology of the cardan joint, but only to an *equivalent* RCCC linkage. It is well known that the cardan joint is an overconstrained linkage and that, in such cases, joint reactions can be reliably computed only by taking into account the elasticity effects. For instance, reference [6] reports on the influence of the intermediate shaft elasticity on the overall performances of the double cardan joint as well as a simplified model for vibration analysis. Moreover in [7], using a model with lumped elasticity, mass and inertia, the analysis of the system was performed with a flexible multibody approach. The results emphasize that both torque and bearing reactions are altered by the shaft stiffness and are related to the the angular velocity.

Purpose of this investigation is the improvement of current dynamic models in the field of transmission joints.

In this paper are presented methods for the following analyses:

*Corresponding author. E-mail: pennestri@mec.uniroma2.it

- static force analysis of the Cardan joint;
- mechanical efficiency analysis of the Cardan joint and the double Cardan homokinetic joint;
- dynamic analysis of the double Cardan homokinetic joint taking into account the inertia of the links;
- fatigue analysis.

Since the above mentioned analyses are significant and iteratively executed during the design cycle of Cardan joints, for completeness, they are all presented in the same paper.

This paper reports a closed form solution of the torque analysis problem in a double Cardan joint under both static and dynamic conditions. In the past a similar analysis was described by F. Duditza[8], but was limited to static conditions. One of the the models described in this paper includes the effects of inertia on torque fluctuation.

This paper reports an original improvement over the method of Morecki for the evaluation of the mechanical efficiency of Cardan and double Cardan homokinetic joints. The previous model, the only one available in technical literature, considered the losses in the bearings connecting the cross with the yokes. The model proposed in this paper includes also the losses in the fixed bearings. It is worth to be noticed that the our method, when these losses are excluded, give the same results obtained with the Morecki's model. Design charts are reported to summarize all the results and easy of use.

Finally, the main purpose of the procedure for fatigue analysis herein presented is also the ascertainment of the influence of working parameters (torque, speed, angular misalignment) on the life expectancy of the joint. The criterion used is an adaptation of the one reported in the ANSI/AGMA norm [17].

2 Brief review of previous contributions on torque analysis

At the book level, the most relevant sources of informations on the Cardan joint are the monograph authored by F. Duditza [8] and the handbook edited by E.R. Wagner [9]. The book of Duditza, originally published in 1966 and translated in many languages, contains the description of different mathematical models for kinematic, dynamic, vibrational and stress analysis of polycardan mechanisms.

Although the kinematics seems extensively studied, the literature on the models for internal forces analysis seems sparse. The first studies on the dynamics of

the cardan joint appear around 1930-1940 and may have been prompted by the numerous joint failures observed in the drivelines of automobiles. These studies hinted the presence of *rocking torques* or *secondary couples*, with direction orthogonal both to input and output shafts, as causes of the failures. Refined models of static analysis, based on the use of the algebra of dual numbers and dual matrices [1, 10], confirmed the findings. Investigations concerned with joint vibration can be found in references [11, 12].

3 Nomenclature

- D : distance between the bearings of the cross;
- d_i : diameter of shaft i ;
- f : friction coefficient;
- I_{ix}, I_{iy}, I_{iz} : principal moment of inertia of the i^{th} body;
- L_i : distance of supports at the i^{th} revolute joint;
- M_{ik} : torque acting from the i^{th} to the k^{th} body;
- M_a, M_u : applied and resisting torques;
- P_{fA}, P_{fB} : powers instantaneously dissipated at the joints connecting the yokes with the cross;
- $[T_{ij}]$: transform matrix;
- $\vartheta_1, \vartheta_3, \vartheta_5$: angular positions of input, intermediate and output shafts (see figure 13);
- $x_i y_i z_i$: moving cartesian system attached to the i^{th} body (see figure 8)
- $X_k Y_k Z_k$: fixed cartesian system associated to the k^{th} body (see figure 8);
- α_i : angular dimension of the link i , measured according to the Denavit-Hartenberg convention;
- β : angle between the input and output shaft in a Cardan joint;
- η_i, η_m : instantaneous and, respectively average, mechanical efficiency of a Cardan joint;

- η_i^{dc}, η_m^{dc} : average mechanical efficiency of the homokinetic double Cardan joint;
- ϕ_{12}, ϕ_{32} : relative angular position of the plane of the cross w.r.t. the planes containing the input and output yoke, respectively;
- ω_i : angular velocity of the i^{th} body, measured in the cartesian system $o - x_i y_i z_i$;
- θ_i : relative angular positions of the links measured according to the Denavit-Hartenberg convention (see Figure 4);
- θ_{1o} : angular position of input link measured w.r.t. vertical plane containing the input shaft;
- $\tau_f^{(i)}$: frictional torque at the i^{th} revolute joint;

Dots denote differentiation w.r.t. time.

4 The Morecki's model for the mechanical efficiency analysis of the Cardan joint

This model¹ is based on the following hypotheses:

- the presence of friction does not alter link equilibrium;
- friction losses concentrated only at the revolute joint at the coupler link;
- negligible inertia;
- absence of manufacturing errors.

The average mechanical efficiency η_m is

$$\eta_m = \frac{1}{2\pi} \int_0^{2\pi} \eta_i d\theta_{1o} = 1 - \frac{2f}{\pi} \cdot \frac{d}{D} \left(\ln \frac{1 + \sin \beta}{\cos \beta} + \tan \beta \right). \quad (1)$$

The Figures 2 and 3 show, respectively, the graphs of the average mechanical efficiencies for the Cardan joint and for the homokinetic double Cardan joint .vs. the adimensional parameter

$$a = \frac{2f}{\pi} \cdot \frac{d}{D} \quad (2)$$

¹The authors could not have access to the original paper "Badanie sprawności mechanicznej i sity wzduznej podwójnych przegubow universalnych Cardana" authored by A. Morecki in 1962. The main equations have been obtained from the book of F. Duditz [8].

The average mechanical efficiency of the homokinetic double Cardan joint is obtained by means of the following formula

$$\eta_m^{dc} = \frac{1}{2\pi} \int_0^{2\pi} \eta_i(\theta_{1o}) \eta_i\left(\theta_{1o} + \frac{\pi}{2}\right) d\theta_{1o} \quad (3)$$

5 The proposed model for the mechanical efficiency analysis of the Cardan joint

Our approach shares the same hypotheses with the Morecki's method. However, the effects of friction on the frame bearings are included.

In this section the expressions for computing the torques at the joints are deduced first, then a simple model for the computation of power losses in the joints is presented. Finally, making use of this model, the average mechanical efficiencies for the Cardan joint and for the homokinetic double Cardan joint are estimated.

5.1 Kinematic analysis of the spherical four-bar linkage

Let us introduce, for each revolute joint, a cartesian frame is introduced according to the well known Denavit-Hartenberg notation [13, 14, 4] (See Figure 4).

From the kinematic analysis of the Cardan joint with this method one readily obtains [4]

$$\theta_2 = \text{ATAN2}(\cos \theta_1 \sin \theta_4 + \cos \alpha_4 \sin \theta_1 \cos \theta_4, \sin \alpha_4 \cos \theta_4) , \quad (4)$$

$$\theta_3 = \text{ATAN2}(\sin \theta_1 \cos \theta_4 + \cos \alpha_4 \cos \theta_1 \sin \theta_4, \sin \alpha_4 \cos \theta_1) , \quad (5)$$

with θ_1 and α_4 imposed and θ_4 computed by solving the nonlinear equation

$$\sin \theta_1 \sin \theta_4 - \cos \alpha_4 \cos \theta_1 \cos \theta_4 = 0 . \quad (6)$$

5.2 Static analysis of the spherical four-bar linkage

From the torque equilibrium condition, applied to all the three moving links, the following system of equations can be deduced [1, 4]:

$$M_{1x} = 0 , \quad (7a)$$

$$M_{1y} + M_{2x} \sin \theta_2 + M_{2y} \cos \theta_2 = 0 , \quad (7b)$$

$$M_{1z} - M_{2x} \cos \theta_2 + M_{2y} \sin \theta_2 = 0 , \quad (7c)$$

$$M_{2x} = 0 , \quad (7d)$$

$$M_{2y} + M_{3x} \sin \theta_3 + M_{3y} \cos \theta_3 = 0 , \quad (7e)$$

$$M_{2z} - M_{3x} \cos \theta_3 + M_{3y} \sin \theta_3 = 0 , \quad (7f)$$

$$M_{3x} + M_{4z} = 0 , \quad (7g)$$

$$M_{3y} + M_{4x} \sin \theta_4 + M_{4y} \cos \theta_4 = 0 , \quad (7h)$$

$$M_{3z} - M_{4x} \cos \theta_4 + M_{4y} \sin \theta_4 = 0 , \quad (7i)$$

The solution of such system, taking into account the results of the kinematic analysis and under the hypothesis that $M_{2z} = M_{3z} = 0$, gives the following expressions:

$$M_{1x} = 0 , \quad (8a)$$

$$M_{1j} = \frac{M_{1z}}{\tan \theta_2} = M_{1z} \tan \alpha_4 \sin \theta_1 \quad (8b)$$

$$M_{2x} = 0 , \quad (8c)$$

$$M_{2y} = -\frac{M_{1z}}{\sin \theta_2} = -M_{1z} \sqrt{1 + \tan^2 \alpha_4 \sin^2 \theta_1} , \quad (8d)$$

$$M_{3x} = \frac{\sin \theta_3}{\sin \theta_2} M_{1z} = \frac{\tan^2 \theta_1 + \cos^2 \alpha_4}{\cos \alpha_4 (1 + \tan^2 \theta_1)} M_{1z} , \quad (8e)$$

$$M_{3y} = -\frac{\cos \theta_3}{\sin \theta_2} M_{1z} = \tan \alpha_4 \cos \theta_1 \sqrt{\sin^2 \theta_1 + \cos^2 \theta_1 \cos^2 \alpha_4} , \quad (8f)$$

$$M_{4x} = \frac{\cos \theta_3 \sin \theta_4}{\sin \theta_2} M_{1z} = \sin \alpha_4 \cos^2 \theta_1 M_{1z} , \quad (8g)$$

$$M_{4y} = \frac{\cos \theta_3 \cos \theta_4}{\sin \theta_2} M_{1z} = \frac{\tan \alpha_4 \sin 2\theta_1}{2} M_{1z} , \quad (8h)$$

$$M_{4z} = -\frac{\sin \theta_3}{\sin \theta_2} M_{1z} = -\frac{\tan^2 \theta_1 + \cos^2 \alpha_4}{\cos \alpha_4 (1 + \tan^2 \theta_1)} M_{1z} . \quad (8i)$$

5.3 Modeling of friction in revolute joints

The frictional forces at the i th revolute joint arise from two sources :

- reaction forces F_{ix} , F_{iy} and F_{iz} ;
- reaction moments M_{ix} and M_{iy}

As a result of our previous static forces analysis, the resultant of the reaction force at the joints is equal zero. However, the resistant action arising from the reaction moment M_{ix} and M_{iy} can be modeled [15, 16] according to the scheme presented in Figure 5.

In particular, for our purposes, the torque M_{ix} is substituted by two parallel and opposite forces F acting normally to the revolute joint axis. Because of the presence of friction, these forces generate the frictional torque

$$\tau_f^{ix} = f \frac{d_i}{L_i} M_{ix} , \quad (9)$$

where d_i is the diameter of the journal bearing, L_i the distance between bearing supports² and f the friction coefficient.

Similarly, the torque M_{iy} generate the frictional torque

$$\tau_f^{iy} = f \frac{d_i}{L_i} M_{iy} . \quad (10)$$

Thus, the resultant frictional torque is

$$\tau_f^{(i)} = f \frac{d_i}{L_i} \sqrt{M_{ix}^2 + M_{iy}^2} . \quad (11)$$

It is clear that the presence of this torque alter the equilibrium of the links. The new reaction torques could be computed by letting $M_{1z} \rightarrow M_{1z} - \text{sign}(\dot{\theta}_1) \tau_f^{(1)}$, $M_{2z} \rightarrow -\text{sign}(\dot{\theta}_2) \tau_f^{(2)}$, $M_{3z} \rightarrow -\text{sign}(\dot{\theta}_3) \tau_f^{(3)}$, $M_{4z} = M_{4z} - \text{sign}(\dot{\theta}_4) \tau_f^{(4)}$ and iteratively solving system (7). The iteration is stopped when all the values of the reaction torques converge. However, in our computations such iteration has not been implemented.

5.4 Mechanical efficiency analysis

The Morecki's model consider only the losses in the revolute joints connecting the cross with the two forks. Thus, identical results (see Figure 2) are obtained when the following definition of mechanical efficiency

$$\eta_m = 1 - \frac{1}{2\pi} \int_0^{2\pi} \frac{|\tau_f^{(2)} \omega_2| + |\tau_f^{(3)} \omega_3|}{M_{1z} \omega_1} d\theta_1 \quad (12)$$

²For a single support bearing, L_i represents the length of the bearing.

is applied and $d_2 = d_3 = d$, $L_2 = L_3 = D$.

The proposed model more realistically includes also the power losses $\tau_f^{(1)}\omega_1$ and $\tau_f^{(4)}\omega_4$ in the joints connecting the forks with the frame.

The average mechanical efficiency of a Cardan joint is computed by means of the following expression

$$\eta_m = 1 - \frac{1}{2\pi} \int_0^{2\pi} \frac{\sum_{i=1}^4 \left| \tau_f^{(i)} \omega_i \right|}{M_{1z} \omega_1} d\theta_1 \quad (13)$$

The values of L_1 , d_1 and L_4 , d_4 must be chosen according to the type of bearings adopted.

The curves shown in Figure 6 illustrate the mechanical efficiency of a Cardan joint computed according to equation (13) and when $L_i = D$, $d_i = d$ ($i = 1, 2, 3, 4$) is assumed.

Similarly, the curves of the mechanical efficiency for the homokinetic Cardan joint, with no bearings on the intermediate shaft, are shown in Figure 7

6 Torque analysis with inertia effects

The proposed analysis of torques in a double cardan joint is based on the following hypotheses

- rigid bodies;
- absence of dissipative effects, manufacturing and/or mounting defects;
- input, intermediate and output shafts are connected with the frame with revolute joints;
- constant angular velocity of the input shaft.

To find the torques acting on each link, the Newton-Euler equations for the motion of a rigid body with a fixed center of mass are applied. Assuming the cartesian axes being principal axes, we obtain:

- Input shaft (Link 1)

$$M_a + M_{21x} = I_{1x} \dot{\omega}_{1x} \quad (14)$$

- First cross (Link 2)

$$M_{12x} + M_{32x} = I_{2x} \dot{\omega}_{2x} + \omega_{2y} \omega_{2z} (I_{2z} - I_{2y}) \quad (15)$$

$$M_{12y} + M_{32y} = I_{2y} \dot{\omega}_{2y} + \omega_{2z} \omega_{2x} (I_{2x} - I_{2z}) \quad (16)$$

$$M_{12z} + M_{32z} = I_{2z} \dot{\omega}_{2z} + \omega_{2x} \omega_{2y} (I_{2y} - I_{2x}) \quad (17)$$

- Intermediate shaft (Link 3)

$$M_{23x} + M_{43x} = I_{3x}\dot{\omega}_{3x} \quad (18)$$

- Second cross (Link 4)

$$M_{54x} + M_{34x} = I_{4x}\dot{\omega}_{4x} + \omega_{4y}\omega_{4z} (I_{4z} - I_{4y}) \quad (19)$$

$$M_{54y} + M_{34y} = I_{4y}\dot{\omega}_{4y} + \omega_{4z}\omega_{4x} (I_{4x} - I_{4z}) \quad (20)$$

$$M_{54z} + M_{34z} = I_{4z}\dot{\omega}_{4z} + \omega_{4x}\omega_{4y} (I_{4y} - I_{4x}) \quad (21)$$

- Output shaft (Link 5)

$$M_{45x} + M_u = I_{5x}\dot{\omega}_{5x} \quad (22)$$

Under our hypotheses, revolute joints cannot transmit torques. Thus the following equalities must hold: $M_{32y}=M_{12z}=M_{34y}=M_{54z}=0$. Moreover, the following transforms must be taken into account (see Appendix) $\{M_{45}\} = -[T_{45}]\{M_{54}\}$, $\{M_{21}\} = -[T_{21}]\{M_{12}\}$, $\{M_{23}\} = -[T_{23}]\{M_{32}\}$, $\{M_{43}\} = -[T_{43}]\{M_{34}\}$. Once the kinematics and the resisting torque M_u are specified, we obtain a linear system of equations where the unknowns are the components of all the eight shaking moments considered plus the applied torque M_a . Since the matrix is sparse, the system of equations can be easily solved by hand.

The numerical data for this example, in SI units, are as follows: $M_u=750$, $I_{1x}=I_{5x}=0.01528$, $I_{2y}=I_{4y}=I_{2z}=I_{4z}=0.00111$, $I_{2x}=I_{4x}=0.00202$.

The plots of the applied torque M_a are shown in Figure 9 for different angular speeds of the driving shaft and shaft misalignment.

7 Stress and fatigue analysis of the double Cardan homokinetic joint

The double Cardan joint was modelled by means of tetraedric solid elements according to the mesh shown in Figure 10

The model was obtained splitting the joint in five bodies: two flanges, two cross journals and a central shaft³. The link journal bearings were modelled introducing rigid elements that allow the rotation. For each body a proper reference system was defined in order to assembly the whole model in the different operating configurations by modifying only the location of this complying with the topological congruence of the joint. For this purpose a numerical code was developed, named KINEJOINT, able to assembly automatically the real configuration of the model for the different angular position analysed.

³The datafile containing the meshed geometry of the joint can be obtained upon request.

The first step of the analysis was to check the modal behaviour of the joint as the static approach used in the force evaluation is valid if the possible dynamic excitation is far from the resonances. Though the modes depend from the angular position and from the cocking angle, for the double cardan joint arrangement analysed, the first mode is always about 1000 Hz while the main excitation is about 100 Hz. This fact assures that no dynamic amplification occurs and that the static approach used is valid. Using the KINEJOINT code, with the graphical interface, the analysis was executed varying:

- angular speed
- torque
- misalignment angle β between driving and driven shaft.

The finite element model gave the results expressed as displacements, strains and stresses. With these it was possible to perform the fatigue stress verification using the formula suggested by the ANSI/AGMA norm

$$\left(\frac{S_a}{S_f}\right)^2 + \left(\frac{S_m}{S_y}\right)^2 = \left(\frac{1}{F_{sy}}\right)^2 \quad (23)$$

where

- F_{sy} Safety fatigue factor;
- S_a Von Mises alternate stress;
- S_e Von Mises equivalent stress;
- S_f Fatigue modified limit;
- S_m Von Mises average stress;
- S_y Yield stress.

For the fatigue modified limit we adopted the expression

$$S_f = S_{fe} \cdot k_a \cdot k_b \cdot (K_t \cdot k_f) \quad (24)$$

where

- k_a Roughness factor;
- k_b Size factor;

- $k_f = 1/K_f$ where K_f is the fatigue stress concentration factor;
- K_t Stress concentration factor;
- S_{fe} Fatigue limit for alternate stress at $2 \cdot 10^6$ cycles;

Making use of K_f definition, it is possible to write [18]

$$\frac{K_f - 1}{K_t - 1} = \frac{1}{1 + \frac{a}{r}} . \quad (25)$$

In the equation above a is a material constant depending on the ultimate static stress and r is the size of the notch.

Since the computations have been carried out by means of a finite elements model, the value of K_t cannot be obtained in the classical way. However, from equation (25) one can infer that $K_t \cdot k_f \geq 1$. Thus, in our calculations, for the favor of safety, it has been assumed $K_t \cdot k_f = 1$.

The material used was 38NiCrMo4 (UNI 5332) with the mechanical properties summarized in the Table 1

Table 1: Summary of the material properties

S_{fe} (MPa)	S_s (MPa)	k_a	k_b	S_f (MPa)
590	850	0.80	0.95	521

Computing average and alternate stresses, respectively, by means of the equations

$$S_m = \frac{S_{eq\min} + S_{eq\max}}{2} , \quad (26a)$$

$$S_a = \frac{S_{eq\min} - S_{eq\max}}{2} , \quad (26b)$$

one can obtain the results summarized in the Table 2 and Figures 11 and 12.

8 Conclusions

This paper presented different analytical tools and procedures to be used for ascertaining the influence of the main working parameters (rotation speed, angular misalignment, transmitted torque) on the kinematic, dynamic and structural performances of the joint.

Table 2: Summary of the numerical results used for the computation of the safety fatigue factor F_{sy}

ω_2 rpm	Torque Nm	β deg	S_{\max} MPa	S_{\min} MPa	S_m MPa	S_a MPa	F_{sy}
6,000	150	5	24.5	23.3	23.9	0.60	35.52
6,000	150	7	25.1	22.7	23.9	1.20	35.40
6,000	150	10	26.0	21.5	23.7	1.25	35.26
4,000	150	5	15.5	14.6	15.0	0.45	56.39
4,000	150	7	15.7	14.4	15.0	0.65	56.29
4,000	150	10	16.0	13.8	14.9	1.10	56.49
6,000	200	5	27.5	26.0	26.75	0.75	31.73
6,000	200	7	27.8	25.8	26.8	1.00	31.64
6,000	200	10	29.0	24.3	26.6	2.35	31.46
5,000	150	5	19.2	18.4	18.8	0.40	45.17
5,000	150	7	19.5	18.0	18.7	0.75	45.20
5,000	150	10	19.8	17.5	18.6	1.15	45.27

It has been shown that the amplitude of torque variations due to the inertia effects, is more affected by the rotation speed than by the angular misalignment β between shafts.

As far as fatigue analysis is concerned, a code has been developed for the purpose of stress analysis by means of finite elements models. These models have shown that the critical region is near the holes of yokes.

The application of ANSI/AGMA norm criterion has shown that increasing rotational velocity causes an assessed-life reduction more than increasing angular misalignment or increasing transmitted torque. This can be clearly observed in the graphs of Figures 11 and 12. This can be explained considering that higher rotational velocity increases the alternate stress rate which reduces F_{sy} more than the increasing of mean stress caused by higher torque. Also an higher angular misalignment β increases the alternate stress rate but in the usual working range (0 - 10 deg) this effect is not so relevant as that of changing rotational velocity.

References

- [1] Fischer, I., Freudenstein, F., Internal Force and Moment Transmission in a Cardan Joint with Manufacturing Tolerances, *ASME Journal of Mechanisms, Transmissions and Automation in Design*, vol.106, December 1984, pp.301-311.
- [2] Chen, C.K., Freudenstein, F., Dynamic Analysis of a Universal Joint with Manufacturing Tolerances, *ASME Journal of Mechanisms, Transmissions and Automation in Design*, vol.108, December 1986, pp.524-532.
- [3] Freudenstein, F., Macey, J.P., The Inertia Torques of the Hooke Joint, *Proc. Of the 21st Biennial ASME Mechanisms Conference*, Chicago, September 16-19, 1990, DE-Vol.24, pp.407-413.
- [4] Fischer, I., *Dual-Number Methods in Kinematics, Statics and Dynamics*, CRC Press, Boca Raton, FL, 1999.
- [5] Dodge, A.Y., Bearing Loads Due to Universal Joint Action, *Automotive Industries*, vol.83, 1940, pp.636-639, 654.
- [6] Biancolini, M.E., Brutti, C., Pennestrì, E., An integrated approach to the dynamic analysis of double cardan joint, *Proc. Sixth Applied Mechanisms and Robotics Conference*, December 12-15 1999, Cincinnati, OH, Paper No. AMR99-035.

- [7] Brutti, C., Pennestrì, E., Biancolini, M.E., On the dynamics of the transmission with a double cardan joint, *Proc. X IFToMM Congres*, 1999, Oulu, Finland, pp.1393-1398.
- [8] Duditzza, F., *Transmissions par Cardan*, Editions Eyrolles, Paris, 1971.
- [9] Wagner, E.R., Cooney, C.E., Cardan or Hooke Universal Joint, in *Universal Joint and Driveshaft Design Manual*, Society of Automotive Engineers, Warrendale, PA, 1979, pp.39-75.
- [10] Yang, A.T., Static Force and Torque Analysis of Spherical Four-Bar Mechanisms, *ASME Journal of Engineering for Industry*, vol.87, 1965, pp.221-227.
- [11] Rosenberg, R.M., On the Dynamical Behavior of Rotating Shafts Driven by Universal (Hooke) Couplings, *ASME Journal of Applied Mechanics*, 1958, pp.47-51.
- [12] Sheu, P.P., Chieng, W.H., Lee, A.C., Modeling and Analysis of the Intermediate Shaft Between Two Universal Joints, *ASME Journal of Vibration and Acoustics*, vol.118, January 1996, pp.88-99.
- [13] Denavit, J., Hartenberg, R.S., A Kinematic Notation for Lower Pair Mechanisms Based on Matrices, *ASME Journal of Applied Mechanics*, vol.77, 1955, pp.215-221.
- [14] Denavit, J., Hartenberg, R.S., *Kinematic Synthesis of Linkages*, McGraw-Hill Book Co., New York, 1964, pp.347-355.
- [15] Shih, C.W., Shih, M. Y., Haug, E.J., Dynamics of Mechanical Systems with Coulomb Friction, Stiction, Impact and Constraint Deletion - III, *Mechanism and Machine Theory*, vol.21, 1986, pp.417-425.
- [16] Dhanaraj, C., Sharan, A.M., Efficient Modeling of Rigid Link Body Dynamic Problems with Friction, *Mechanism and Machine Theory*, vol.30, 1995, pp.749-764.
- [17] ANSI/AGMA Norm 6001-D97
- [18] Petereson, R.E. *Stress Concentration Factors*, John Wiley & Sons, New York, 1974.
- [19] Barone, S., Bruno, P., Calì, C., Citarella, R., Robust design and simulation for the multiobjective optimization of a joint, *Proc. XXIX Congress AIAS*, Lucca - Italy, September 2000, pp.915-924. (*in italian*)

[20] Buch, A. *Fatigue Strength Calculation*, Trans. tech Pub. USA 1988.

Appendix

The following matrices define the transformations between the different cartesian reference system ($c_i = \cos \vartheta_i$, $s_i = \sin \vartheta_i$, $c_{\beta k} = \cos \beta_k$, $s_{\beta k} = \sin \beta_k$) (See Figure 13).

$$\begin{aligned}
 [T_{21}] &= \begin{bmatrix} -s_1 c_3 c_{\beta 1} - s_3 c_1 & -c_3 s_{\beta 1} & 0 \\ s_1 c_3 s_{\beta 1} & -c_3 c_{\beta 1} & c_1 \\ -c_1 c_3 s_{\beta 1} & s_3 & s_1 \end{bmatrix}, & [T_{13}] &= \begin{bmatrix} c_{\beta 1} & -s_{\beta 1} & 0 \\ s_{\beta 1} & c_{\beta 1} & 0 \\ 0 & 0 & 1 \end{bmatrix}, \\
 [T_{45}] &= \begin{bmatrix} -s_5 c_3 c_{\beta 2} - s_3 c_5 & -c_3 s_{\beta 2} & 0 \\ s_5 c_3 s_{\beta 2} & -c_3 c_{\beta 2} & c_5 \\ -c_3 c_5 s_{\beta 2} & s_3 & s_5 \end{bmatrix}, & [T_{53}] &= \begin{bmatrix} -c_{\beta 2} & s_{\beta 2} & 0 \\ -s_{\beta 2} & -c_{\beta 2} & 0 \\ 0 & 0 & 1 \end{bmatrix}, \\
 [T_{23}] &= [T_{21}] [T_{13}], & [T_{34}] &= [T_{53}]^T [T_{45}]^T.
 \end{aligned}$$

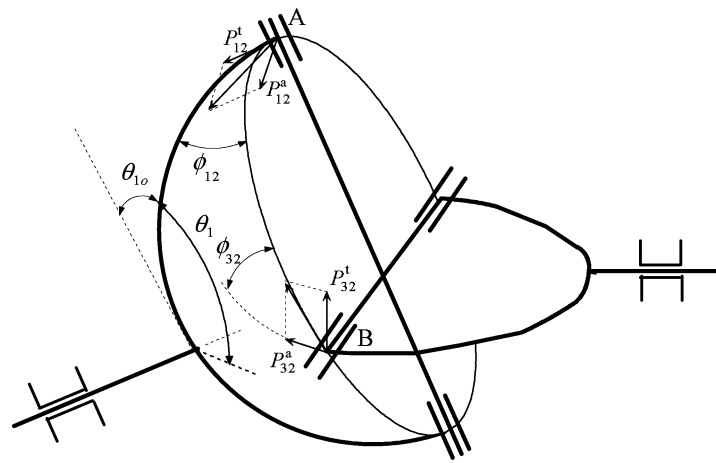


Figure 1: The Morecki's model: Nomenclature

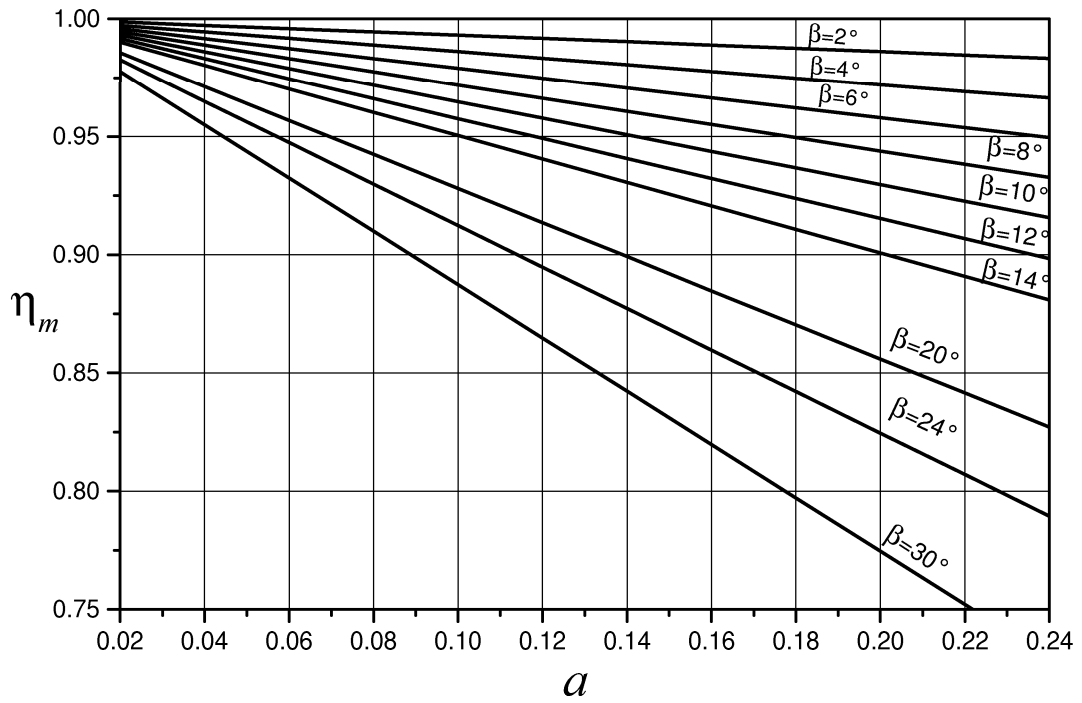


Figure 2: Mechanical efficiency of a Cardan joint according to the Morecki's model

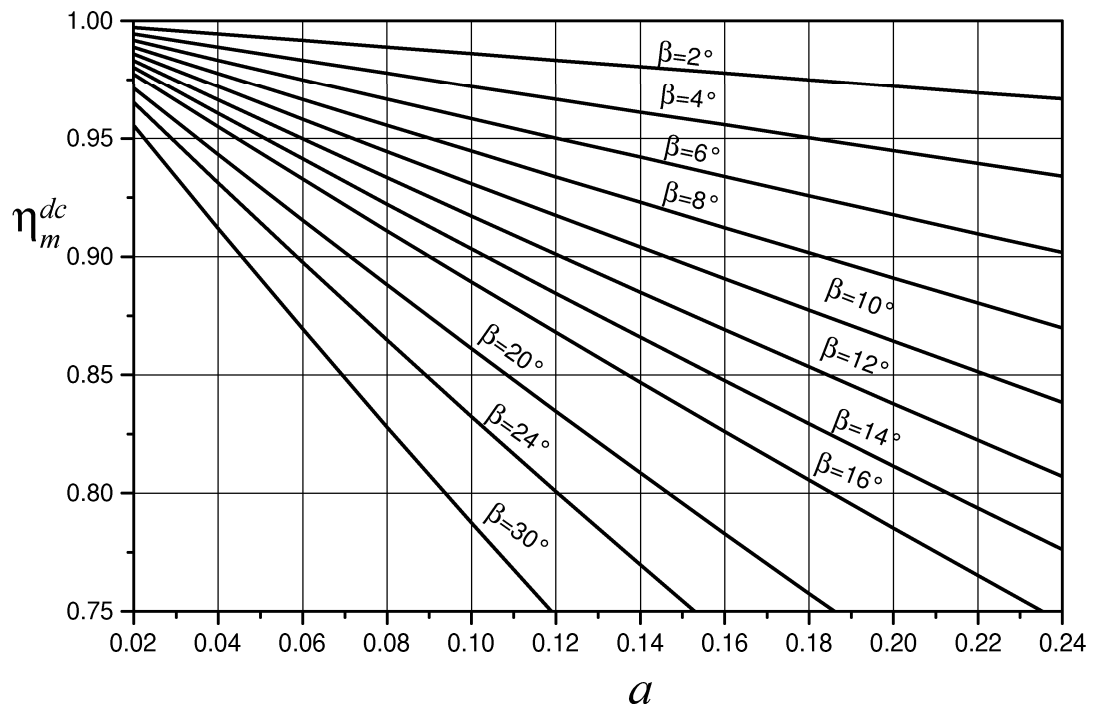


Figure 3: Mechanical efficiency of homokinetic double Cardan joint according to the Morecki's model

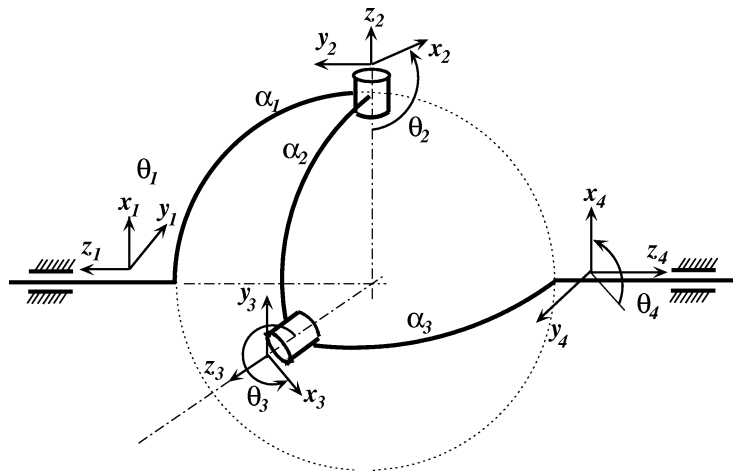


Figure 4: Kinematic analysis of a spherical four-bar linkage by means of the Denavit-Hartenberg method: Nomenclature

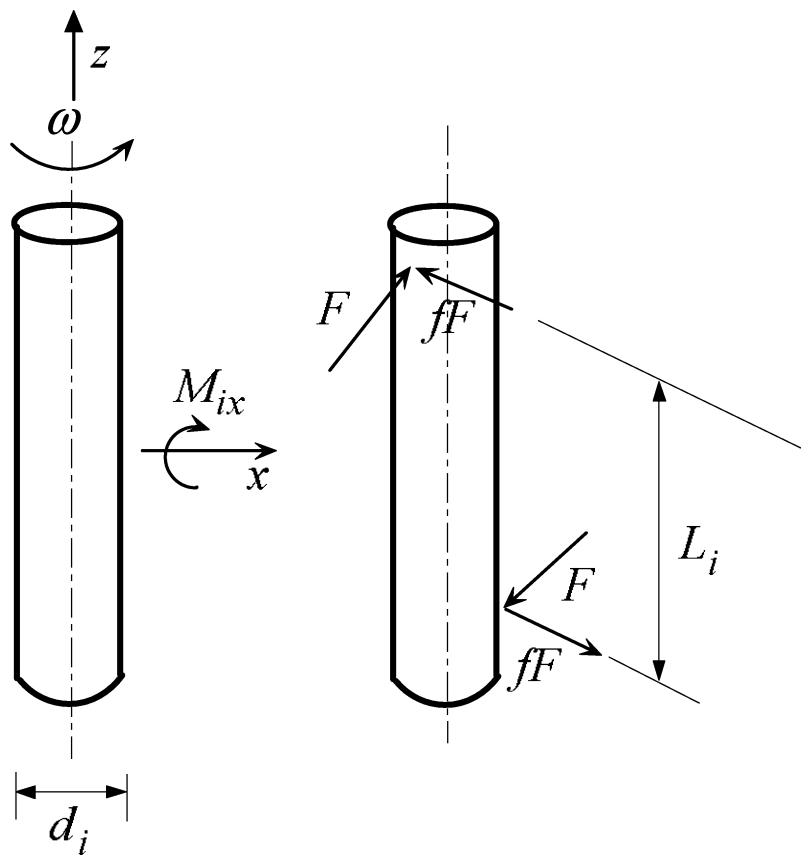


Figure 5: Modeling of friction in the revolute pairs

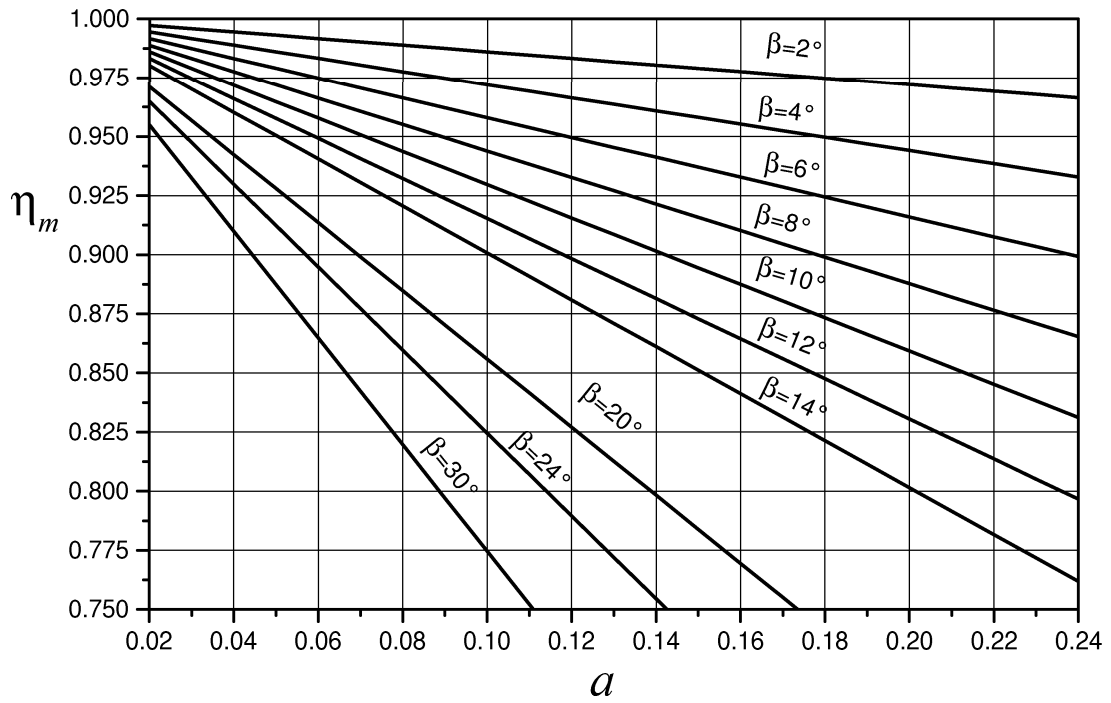


Figure 6: Mechanical efficiency of a Cardan joint according to the proposed model

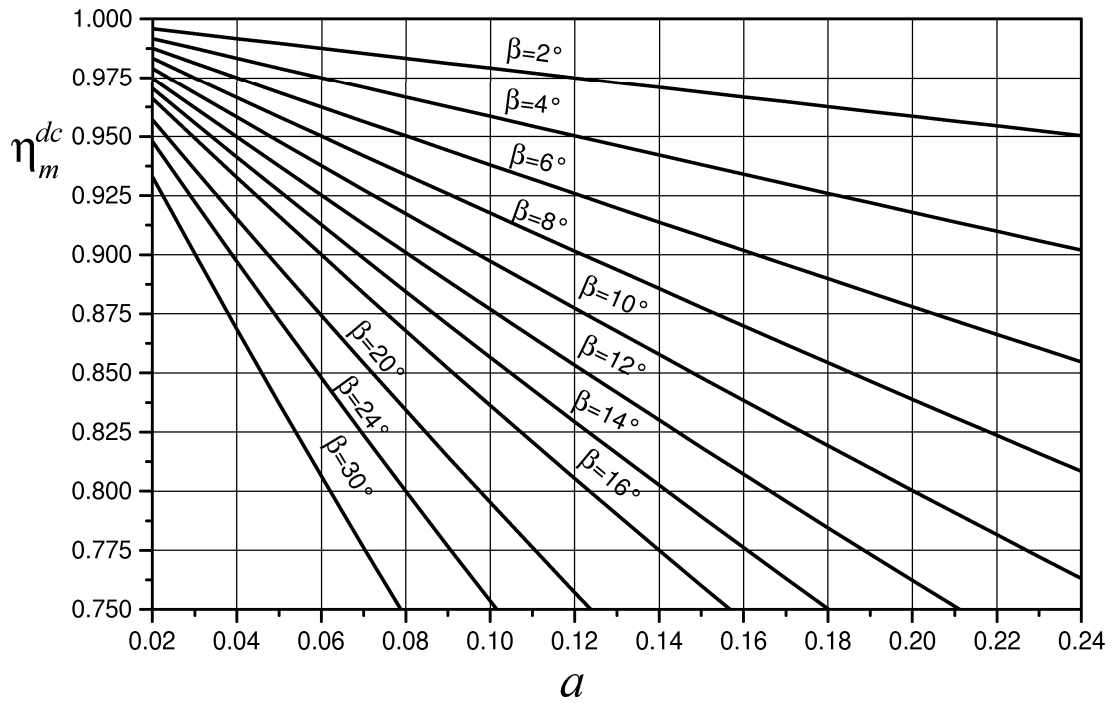


Figure 7: Mechanical efficiency of the homokinetic double Cardan joint according to the proposed model

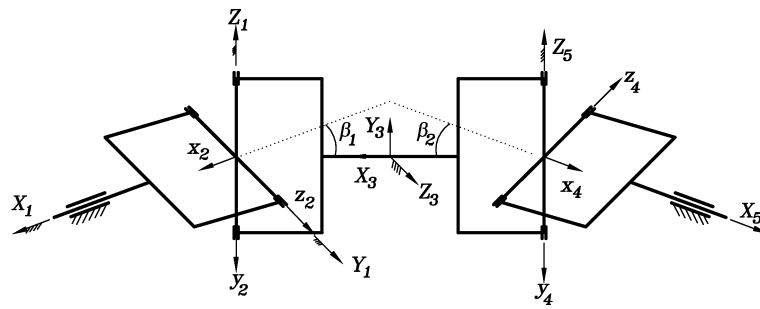


Figure 8: Scheme of an homokinetic double Cardan joint.

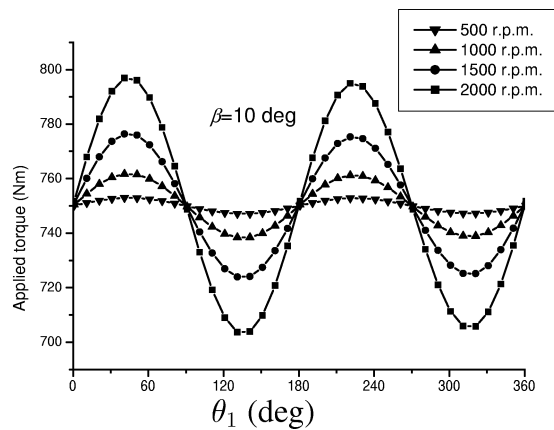
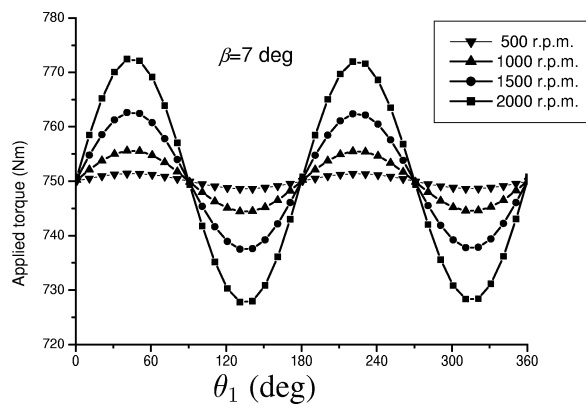
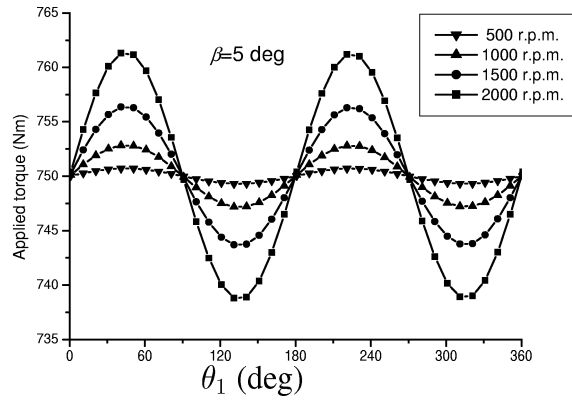


Figure 9: Applied torque vs. angular position and different angular speeds of the driving shaft.

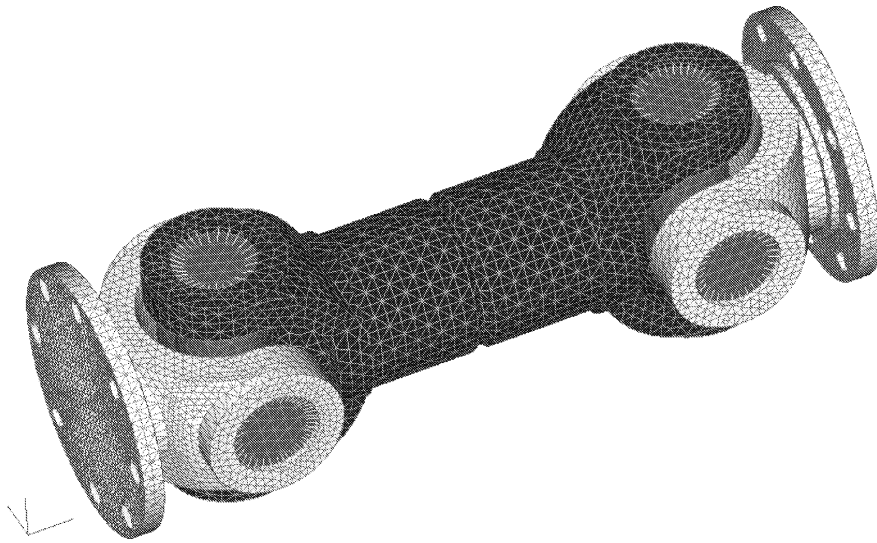


Figure 10: Overall view of the finite element model

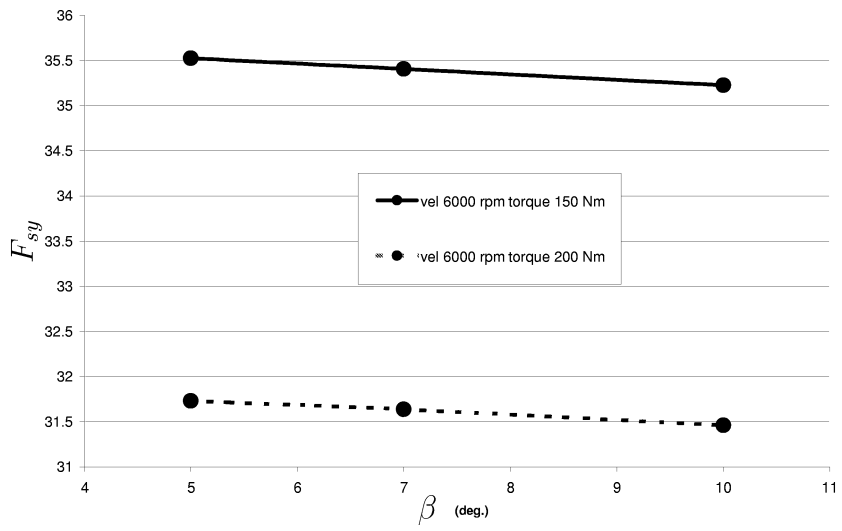


Figure 11: Influence of angular misalignment, angular speed and torque on the safety fatigue factor F_{sy}

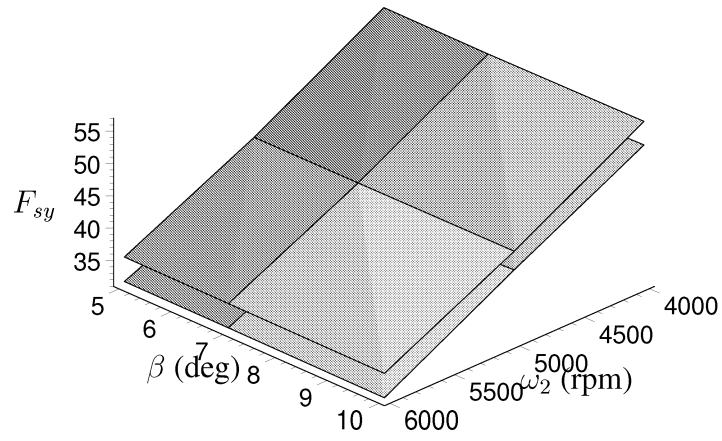


Figure 12: Influence of angular misalignment and torque on the safety fatigue factor F_{sy}

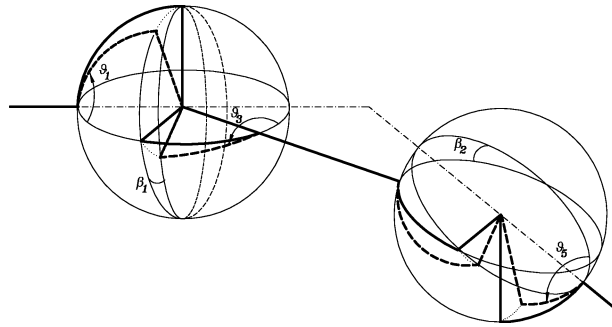


Figure 13: Convention for measuring angular positions of the links.